Proton-Coupled Electron Transfer of an Osmium Aquo Complex on a Self-Assembled Monolayer on Gold

Robert M. Haddox and Harry O. Finklea*

Department of Chemistry, West Virginia University, Morgantown, West Virginia 26506-6045

Received: July 8, 2003; In Final Form: November 14, 2003

A one-electron, one-proton (1*e*1H) redox couple based in an osmium aquo complex is attached to a self-assembled monolayer of alkanethiol on a gold electrode. The formal potential behavior of the Os aquo complex exhibits the expected pH dependence for a 1*e*1H system. The thermodynamic parameters are a formal potential of +0.30 V vs SCE for [Os(II/III)(H_2O)], a formal potential of −0.11 V vs SCE for [Os(II/III)(OH)], a pK_a of 2.4 for [Os(III)(H_2O/OH)], and a pK_a of 9.3 for [Os(II)(H_2O/OH)]. A stepwise electron−proton transfer model, widely used in the electrochemical literature, predicts the effects of pH and overpotential on the kinetics of charge transfer for the 1*e*1H system. The kinetic behavior of the Os aquo complex deviates substantially from the predictions of the stepwise model. In particular, the standard rate constant and the transfer coefficient at zero overpotential are nearly independent of pH over the pH range at which proton-coupled electron transfer occurs, and Tafel plots are asymmetrical (steeper anodic branch) over most of the pH range examined (1−12). Possible double-layer effects caused by the presence of ionizable carboxylate moieties in the monolayer are ruled out by the absence of any pH effects on the formal potential and kinetics of an analogous Os chloride complex. A concerted electron−proton transfer mechanism is hypothesized to explain the observed kinetic behavior.

Introduction

Redox couples attached to self-assembled monolayers on electrodes afford an excellent means of testing theories of electron transfer at electrodes because of their ability to adjust the standard rate constant into an experimentally convenient range, thus allowing measurement of rate constants at large overpotentials. The alkane layer spacer also helps to minimize double-layer effects on the kinetic measurements.[1−21] We are applying this tool to redox couples in which atom transfer is coupled to electron transfer, specifically proton-coupled electron transfer (PCET) systems. These redox couples have the general form

$$\mathbf{O} + n\mathrm{e}^- + h\mathrm{H}^+ \rightleftarrows \mathbf{R} \qquad (1)$$

where **O** and **R** are the oxidized deprotonated form and reduced protonated form, respectively.

Detailed analysis of the kinetics of PCET systems at electrodes are in the literature.[22,23] In particular, Laviron has provided a systematic theoretical treatment of 1*e*1H (one-electron, one-proton), 1*e*2H, 2*e*1H, and 2*e*2H systems.[24−34] Two key assumptions in the treatment are the stepwise transfer of electrons and protons and proton transfer treated as equilibria. These assumptions lead to square, ladder, and picket fence schemes with multiple species varying in oxidation and protonation states. The simplest system, 1*e*1H, yields a square scheme containing (in Laviron's notation) members **O**, **P**, **Q**, and **R**, with **P** being the reduced deprotonated form and **Q** being the oxidized protonated form. In the square scheme, thermodynamic parameters include standard potentials E°_1 (for **Q**/**R**) and E°_2 (for **O**/**P**) and acid dissociation constants K_{a1} (for **O**/**Q**) and K_{a2} (for **P**/**R**), while kinetic parameters include standard rate constants k_{s1} and k_{s2} with transfer coefficients α_1 and α_2 for the electron-transfer steps **Q**/**R** and **O**/**P**, respectively. The following predictions are obtained from the 1*e*1H square scheme model: (a) a pH-dependent formal potential E_r which defines three regimes of low (pH < pK_{a1}), intermediate (pK_{a1} < pH < pK_{a2}), and high pH behavior (pH > pK_{a2}), (b) an apparent standard rate constant k_s at the formal potential E_r which exhibits maximum values at low and high pH (pure electron transfer) and a deep minimum in the intermediate pH regime (Figure 1), and (c) a path of electron transfer (**OPR** or **OQR**) that depends on pH in the intermediate pH regime. These predictions are obtained with the assumption that both transfer coefficients are independent of potential.

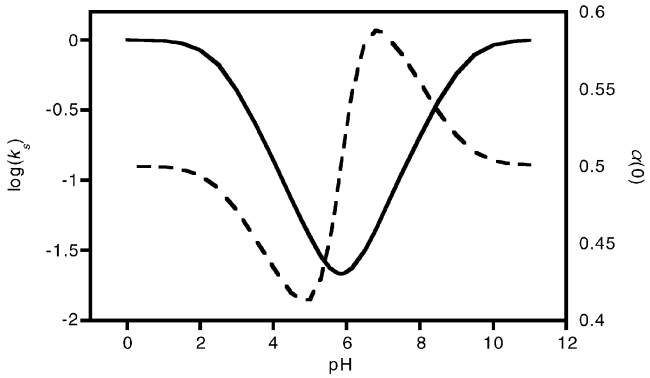

Figure 1. Theoretical curves of log(k_s) (solid line) and α(0) (dashed line) vs pH for a 1*e*1H redox couple from the stepwise model. Parameters are selected to match the data for the osmium aquo comples: pK_{a1} = 2.4, pK_{a2} = 9.3, $k_1 = k_2 = 1\ s^{-1}$. Potential-dependent transfer coefficients are based on reorganization energies (λ) of 0.6 eV for all redox forms.

We have reanalyzed the 1*e*1H system and the more complex systems with the incorporation of potential-dependent transfer

* Corresponding author: e-mail Harry.Finklea@mail.wvu.edu.

10.1021/jp035967e CCC: $27.50
Published on Web 01/09/2004

coefficients.[35,36] The potential dependence is obtained from Marcus density-of-states theory, which has been successful in fitting Tafel plots of simple electron transfer systems. The predicted behavior is qualitatively similar to that given by Laviron. One notable difference is that the apparent transfer coefficient and the path of electron transfer become a function of both potential and pH. In particular, the apparent transfer coefficient at zero overpotential ($E = E_r$), $\alpha(0)$, deviates from 0.5 even though the transfer coefficients for the pure electron transfer steps are 0.5 at the respective standard potentials of the pure electron transfer steps (Figure 1). $\alpha(0)$ is greater than 0.5 for pHs near pK_{a2} (path **OPR**) and less than 0.5 for pHs near pK_{a1} (path **OQR**).

Our goal has been to test the stepwise model predictions using well-defined 1*e*1H systems. While there are a number of reports of PCET redox centers attached to self-assembled monolayers, there has not been a systematic study of the thermodynamic and kinetic behavior of these redox centers as a function of pH.[37−62] We[63,64] have examined the behavior of the 1*e*1H galvinol/galvinoxyl redox center, a system originally reported by Shultz and Tew.[65] Only the high pH thermodynamic ($E°_2$, pK_{a2}) and kinetic parameters (k_{s2}) are accessible for that redox center. As predicted by the stepwise model, $\alpha(0)$ is above 0.5 at pH < pK_{a2}. However, the plot of log(k_s) vs pH deviates significantly above the predicted trend line for pHs below 8. Arguments were made against two possible explanations for the deviation (second coupled proton−electron transfer step, kinetic control by proton transfer). This result has led us to question the validity of stepwise proton-coupled electron transfer model.

Because the low pH behavior is inaccessible for the galvinol redox center, it is highly desirable to investigate another 1*e*1H system that affords access to the entire pH range of behavior. Takeuchi et al.[66,67] reported that the formal potential of [Os(II/III)(tpy)(bpy)(L)] (L = H_2O/OH) (where tpy = 2,2′,2″-terpyridine and bpy = 2,2′-bipyridine) exhibits the expected pH behavior of a 1*e*1H system until, at very high pH, the Os(II/III) wave merges into the Os(III/IV) wave. Both standard potentials and pK_as are accessible in aqueous electrolytes: $E°_1$(**Q/R**) = +0.41 V vs the NaCl-saturated calomel electrode (SSCE), $E°_2$(**O/P**) = +0.09 V vs SSCE, pK_{a1}(**O/Q**) = 2.0, and pK_{a2}(**P/R**) = 7.8. The following identifications are made with Laviron's notation: **O** = [Os(III)(OH)]; **P** = [Os(II)(OH)]; **Q** = [Os(III)(H_2O)]; **R** = [Os(II)(H_2O)]. The synthesis, attachment to monolayers, and electrochemical behavior of analogous redox couples, [Os(II/III)(bpy)$_2$(4-AMP)(L)] (4-AMP = 4-aminomethylpyridine; L = H_2O or Cl), are reported here.

Experimental Section

Synthesis of [Os(II)(bpy)$_2$(4-AMP)(Cl)](PF$_6$) (4-AMP = 4-aminomethylpyridine). Os(bpy)$_2$(Cl)$_2$ was prepared according to the original procedure given by Buckingham et al.[68] Typically, 100 mg of K_2OsCl_6 and 65 mg of 2,2′-bipyridine (2 equiv) were refluxed in anhydrous dimethylformamide for 1 h. After cooling, 20 mL of dilute sodium dithionite solution was added and the mixture chilled. The resulting red-purple crystals were washed with water and diethyl ether. Cyclic voltammetry in 0.1 M tetramethylammonium tetrafluoborate in acetonitrile showed the Os(II/III) wave at −0.19 V vs SCE.

To prepare the 4-AMP substituted product, 100 mg of Os(bpy)$_2$(Cl)$_2$ and 1 equiv of 4-AMP (18 mg) were refluxed in 2 mL of ethylene glycol under argon. To precipitate the product, 2 mL of aqueous saturated NH_4PF_6 was added to the cooled solution. The brown solid was rinsed with water and dried. Cyclic voltammetry in 0.1 M $NaClO_4$ in acetonitrile showed the Os(II/III) wave at +0.20 V vs SCE.

Synthesis of [Os(II)(bpy)$_2$(4-AMP)(H_2O)](PF$_6$). Attempts to prepare the product by heating [Os(II)(bpy)$_2$(4-AMP)(Cl)](PF$_6$) in triflic acid failed because of the formation of multiple products. A pure product could be obtained in two steps from [Os(bpy)$_2$(Cl)$_2$] via the intermediate [Os(bpy)$_2$(CO_3)].[69]

To synthesize [Os(bpy)$_2$(CO_3)], 100 mg of [Os(bpy)$_2$(Cl)$_2$] was dissolved in 15 mL of deionized water, and the solution was saturated with argon to remove oxygen. Sodium carbonate (1 g) was added and the solution refluxed for 2 h. Another 1 g portion of sodium carbonate was added and the solution refluxed for another 2 h. A final 1 g portion of sodium carbonate was added and the solution refluxed for another 2 h. After cooling, the black product was collected by filtration and rinsed with alkaline (pH > 9) water until the rinsings turned from black/purple to brown/red in color. Dissolution of the product in an acidic electrolyte resulted in the immediate conversion of [Os(bpy)$_2$(CO_3)] to [Os(bpy)$_2$(H_2O)$_2$]$^{2+}$. Cyclic voltammetry of the latter product in pH 1.5 electrolyte showed redox waves at +0.06 V vs SCE (Os(II/III)), +0.54 V vs SCE (Os(III/V)), and +0.72 V vs SCE (Os(V/VI)); the interval between the formal potentials are in agreement with literature values.[70]

To prepare [Os(II)(bpy)$_2$(4-AMP)(H_2O)](PF$_6$)$_2$, 100 mg of [Os(bpy)$_2$(CO_3)] was added to 50 mL of deionized water, and the solution was saturated with argon. Five drops of 4-AMP (a large excess) was added and the solution refluxed for 4 h. After cooling, the product was precipitated by the addition of solid NH_4PF_6. The filtered product was washed with water. Controlled potential coulometry showed that this product was 84% pure. Because the carbonate complex hydrolyses to the *cis*-aquo complex, the pyridine and water ligands are likely to be in the *cis* configuration.[70]

The cyclic voltammetry of [Os(II)(bpy)$_2$(4-AMP)(H_2O)](PF$_6$)$_2$ in aqueous electrolyte was consistent with the desired 1*e*1H redox couple of [Os(III)(OH)]/[Os(II)(H_2O)] with the addition of another protonatable site, the pendant amine on the pyridine. The formal potential exhibited the expected −59 mV/pH slope from pH 3 to pH 7 with pH-independent values for pH < 2 and pH > 8. Since the amine has a pK_a close to that of the Os(II) aquo complex, only the low pH parameters were unambiguously identified: $E°_1$ = +0.31 V vs SCE, pK_{a1} = 2.1.

Preparation of the Self-Assembled Monolayers. The preparation of the gold bead electrodes has been described.[63,64] Two distinct monolayers were used to couple the osmium complexes to gold electrodes. For [Os(II)(bpy)$_2$(4-AMP)(Cl)](PF$_6$), monolayers of 16-mercaptohexadecanoic acid (HS(CH$_2$)$_{15}$COOH) were prepared by immersing the gold bead in a dilute (10^{-3} M) solution of the thiol in ethanol overnight. For [Os(II)(bpy)$_2$(4-AMP)(H_2O)](PF$_6$)$_2$, mixed monolayers were prepared by immersing the gold bead electrode overnight in an ethanol solution containing 0.6 mM 12-mercaptododecanol (HS(CH$_2$)$_{12}$OH) and 0.4 mM HS(CH$_2$)$_{15}$COOH. The mixed monolayer was used for the osmium aquo complex because preliminary experiments indicated that the aquo complex was not stable on a 100% HS(CH$_2$)$_{15}$COOH monolayer. A new pH-independent redox wave appeared which was tentatively assigned to a carboxylate complex of the osmium redox center. This instability did not appear on the mixed monolayer.

To couple [Os(II)(bpy)$_2$(4-AMP)(Cl)]$^+$ to the monolayer, 150 mg of 1-ethyl-(3-(dimethylamino)propyl)carbodiimide (EDC) and 150 mg of KNO_3 were dissolved in 20 mL of 5 mM phosphate buffer adjusted to pH 7. To this solution was added

2 mg of $[Os(II)(bpy)_2(4\text{-}AMP)(Cl)](PF_6)$. After saturating the solution with argon, the monolayer-coated electrode was immersed in this solution for 1 h and then immersed in the ethanol deposition solution containing $HS(CH_2)_{15}COOH$ for 1 h to improve the packing of the monolayer (as shown by decreased charging current).

The preceding procedure resulted in an unknown impurity wave when $[Os(II)(bpy)_2(4\text{-}AMP)(H_2O)](PF_6)_2$ was used. The composition of the coupling solution and the reaction time were modified to avoid the appearance of the impurity wave. The electrode coated with the mixed monolayer was immersed for only 15 min in an argon-saturated solution composed of 15 mg of EDC and 2 mg of the osmium complex in 20 mL of pH 7 phosphate buffer (0.1 M). The redox-coupled electrode was stored in pure water until its electrochemical characterization.

In both coupling reactions, conditions were adjusted to achieve redox center coverages of ca. 1×10^{-11} mol/cm^2. This low coverage (5−10% of maximum coverage) was designed to avoid interactions between adjacent redox centers and to minimize the *iR* drop corrections required during data analysis (see below).

Electrochemistry and Data Analysis. The electrochemical cell with SCE and Ir/IrO_2 quasi-reference electrode, electrolyte composition (0.1 M Britton−Robinson buffer + 0.5 M K_2SO_4), pH calibration, cyclic voltammetry sweep rate study, and data analysis have been described.[63,64] Briefly, cyclic voltammetry was performed at each pH for scan rates of 0.01−1000 V/s, and the current−potential data were recorded on a digital oscilloscope. The data analysis included subtraction of the charging current to isolate the faradaic current and correction of the applied potential for *iR* drop. The uncompensated resistance for *iR* drop compensation was measured by high-frequency ac voltammetry. The data analysis yielded the apparent standard rate constant k_s (measured at $E = E_r$) and rate constants k as a function of overpotential η ($= E - E_r$) measured at 50% conversion of the reactant oxidation state to the product oxidation state. Tafel plots ($\ln(k)$ vs η) were fitted to theoretical Tafel curves from the Marcus density-of-states model to extract anodic and cathodic reorganization energies (λ). To obtain $\alpha(0)$, the transfer coefficient was calculated at each overpotential η using the corresponding $\ln(k)$ and an estimated k_s value. A plot of $\alpha(\eta)$ vs η (magnitude of η less than 0.25 V) was fitted by nonlinear optimization (least-squares error) to a straight line to yield the best fit k_s value and the intercept $\alpha(0)$.

Results

Because the coupling chemistry required pendant carboxylic acid groups on the surface of the monolayer, the question arises as to the possible effect of the protonation state of any free COOH groups on the formal potential and the electron transfer rate constants (double-layer effect). Dissociation of the carboxylic acid causes a change in the local electrostatic potential and consequently the driving force for electron transfer; this is one type of double-layer effect on electron transfer kinetics.[71] $[Os(bpy)_2(4\text{-}AMP)(Cl)]^+$ attached to a pure $HS(CH_2)_{15}COOH$ monolayer serves as a control experiment. Ideally, this redox center should exhibit formal potentials and kinetic parameters independent of pH.

Reversible cyclic voltammograms of attached $[Os(bpy)_2(4\text{-}AMP)(Cl)]^+$ exhibit a peak splitting of 25−35 mV and a peak half-width of 120 mV at all pHs. The formal potential is +0.127 ± 0.007 V vs SCE for one monolayer at pHs 2, 4, 6, and 9. Table 1 lists the standard rate constants and anodic and cathodic reorganization energies for kinetic measurements at pHs ranging from 1.5 to 11.0. The mean values are 11 ± 1 s^{-1} for k_s and 0.6 ± 0.1 eV for λ. Clearly, these parameters show no significant trends with respect to pH. Thus, double-layer effects are considered to be negligible. The ionizable COOH moieties on SAM surface appear to have little impact on either the thermodynamics or the kinetics of the Os redox centers, probably because of the high ionic strength of the electrolyte. The standard rate constant is noticeably faster than the standard rate constant for $[Ru(NH_3)_5(4\text{-}AMP)]^{2+}$ tethered to an identical SAM (k_s ca. 1 s^{-1}).[7] The higher standard rate constant for the osmium complex can be rationalized by its smaller reorganization energy of 0.6 eV vs 0.8 eV for the ruthenium complex.[7] The Marcus density-of-states model predicts that this 0.2 eV difference causes an order of magnitude difference in standard rate constants.

TABLE 1: Kinetic Parameters for $[Os(bpy)_2(4\text{-}AMP)(Cl)]$ Monolayers as a Function of pH[a]

pH	k_s/s^{-1}	cathodic λ/eV	anodic λ/eV
1.5	12	0.6	0.65
1.9	8.	0.55	0.7
2.9	11	0.6	0.7
4.3	9.5	0.6	0.65
5.4	13	0.6	0.6
6.5	11	0.55	0.6
7.2	9.9	0.55	0.65
9.1	9.9	0.55	0.65
11.0	9.3	0.55	0.55

[a] Average standard rate constants (k_s) and reorganization energies (λ) from Tafel plots for monolayers with attached $[Os(bpy)_2(4\text{-}AMP)(Cl)]$. The average standard rate constant is 11 ± 1 s^{-1}, the average cathodic reorganization energy is 0.57 ± 0.03 eV, and the average anodic reorganization energy is 0.64 ± 0.05 eV.

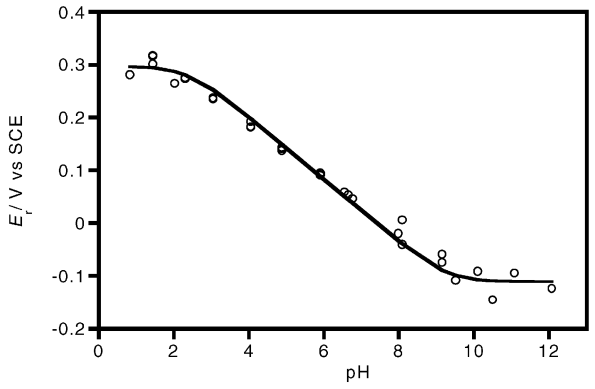

Figure 2. Apparent formal potential E_r vs pH for $[Os(II/III)(bpy)_2(4\text{-}AMP)(H_2O)]$. The circles are experimental values, and the solid line is a least-squares fit to the 1*e*1H stepwise model. Fitted parameters are $E^\circ_1 = +0.30$ V vs SCE, $pK_{a1} = 2.4$, $E^\circ_2 = -0.11$ V vs SCE, $pK_{a2} = 9.3$.

Discussion of the monolayers containing $[Os(II)(bpy)_2(4\text{-}AMP)(H_2O)]^{2+}$ focuses on the Os(II/III) redox wave. The Os(III/IV) redox wave is accessible but is close to the potential at which gold oxidizes, which leads to instability of the monolayer. Reversible cyclic voltammograms of monolayers with attached $[Os(II)(bpy)_2(4\text{-}AMP)(H_2O)]^{2+}$ typically exhibit peak splittings of 5−20 mV and half-widths of 100 mV at all pHs. The reversible formal potential E_r displays the pH dependence anticipated for a 1*e*1H redox center (Figure 2). A least-squares fit to the model yields all four thermodynamic parameters: $E^\circ_1 = +0.30$ V vs SCE, $pK_{a1} = 2.4$, $E^\circ_2 = -0.11$ V vs SCE, $pK_{a2} = 9.3$. These values are in reasonable agreement with the values reported for $[Os(tpy)(bpy)(H_2O)]^{2+}$.[67]

An overlay of cyclic voltammograms at pH 4.0 (Figure 3) illustrates the transformation from reversible behavior to kineti-

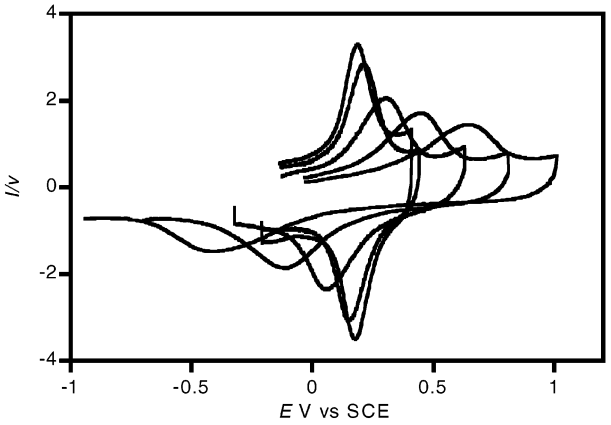

Figure 3. Overlay cyclic voltammograms of [Os(II/III)(bpy)$_2$(4-AMP)-(H$_2$O)] at pH 4.0. The CVs are normalized with respect to the scan rate; the vertical axis units are μA/(V/s). CVs are shown for 0.1, 1, 10, 100, and 1000 V/s.

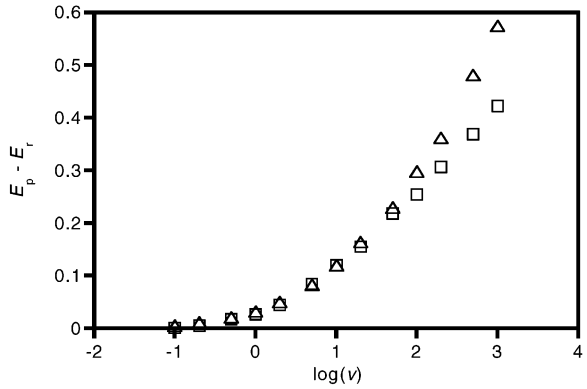

Figure 4. Absolute peak overpotentials as a function of log scan rate at pH 4.0. Anodic (squares) and cathodic (triangles) peak potentials are obtained for the CVs in Figure 3.

cally controlled behavior with increasing scan rates. The peak splitting increases from 5 mV at 0.1 V/s to 1040 mV at 1000 V/s. According to the stepwise model, kinetically controlled cyclic voltammograms should exhibit asymmetry at the pHs which lie between the two pK_a's, except for the pH midway betwen the pK_a's (5.9). Cyclic voltammograms at pH 4.0 should show the pattern for $\alpha(0)$ less than 0.5 (Figure 1): sharp anodic peaks relatively close to the formal potential and broad cathodic peaks relatively far from the formal potential. Figure 4 show the absolute peak overpotentials ($E_p - E_r$) as a function of log scan rate at pH 4.0. At this pH, there is indeed a tendency for cathodic overpotentials to be slightly larger in absolute magnitude than anodic overpotentials at the higher sweep rates, suggesting that $\alpha(0)$ is slightly less than 0.5. However, the same pattern of peak potentials vs log scan rate is observed at all pHs except at pHs between 8 and 10, where the anodic and cathodic peak potential magnitudes are equal at all scan rates.

Figure 5 is a plot of log(k_s) vs pH, where k_s is obtained from kinetically controlled cyclic voltammograms at the formal potential.[63] The theoretical curve is fitted at high and low pH to the measured standard rate constants since those pH ranges should correspond to pure electron transfer. The theoretical curve is calculated assuming $\alpha = 0.5$ at all potentials; this curve is very close to the one expected for potential-dependent transfer coefficient with $\lambda = 0.6$ eV (compare with Figure 1). The data exhibit an average standard rate constant for pure electron transfer of 60 s^{-1} at both high and low pH. These values are higher than the 11 s^{-1} for the chloride analogue with the same tether length. The diluent thiol (HS(CH$_2$)$_{12}$OH) in these mono-

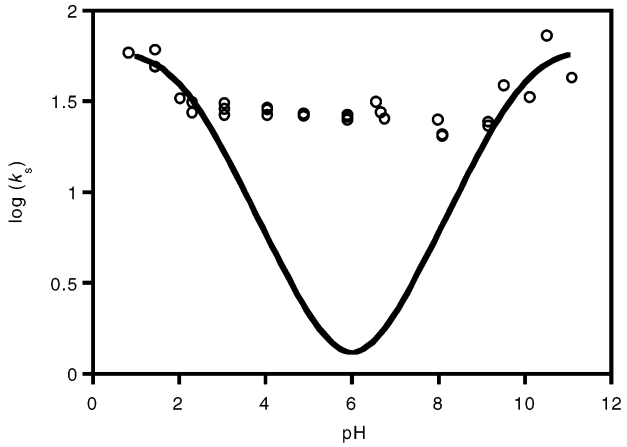

Figure 5. Log(k_s) vs pH. Circles are the k_s values obtained by data analysis at $\eta = 0$ V. The solid line is the expected pH dependence for the stepwise model with the curve approximately fitted to the measured rate constants at low and high pH.

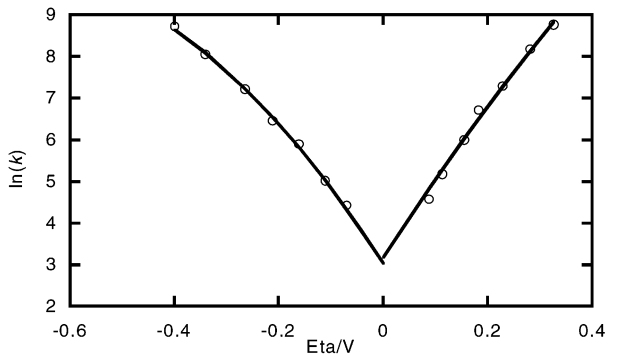

Figure 6. Tafel plot of ln(k_s) vs overpotential η at pH 0.8. The solid line is the least-squares fit to the Marcus density-of-states model with $\lambda = 1.4$ eV for the anodic branch and $\lambda = 0.60$ eV for the cathodic branch. The anodic intercept is 3.17 ($k_s = 24$ s^{-1}), and the cathodic intercept is 3.03 ($k_s = 21$ s^{-1}).

layers is shorter than in the monolayer with the osmium chloride complex, and previous experiments have shown that the standard rate constant is sensitive to the length of noncovalently attached diluent thiols in the monolayer structure.[4] Considerable deviation between the data and predictions of the stepwise model is present at the intermediate pHs. The stepwise model predicts a minimum k_s value of 1.5 s^{-1} at the mid-pH. The observed k_s value, 30 s^{-1}, is 20 times higher.

An examination of all Tafel plots suggests that distinct patterns of kinetic behavior are found in four pH ranges: <2, 2−8, 8−10, and >10. Figures 6 and 7 show two examples of Tafel behavior. All Tafel plots are fitted with reorganization energies of the Marcus DOS theory even though the theory is only valid for pure electron transfer. The fit is a measure of the Tafel curvature; a more curved branch of the Tafel plot yields a lower value of λ. Figure 8 summarizes the reorganization energies for all the pHs. At low pH (Figure 6, pH < 2) and at high pH (>10), Tafel plots are asymmetrical with reorganization energies of 1.0−1.4 eV for the anodic branch (large uncertainty because the overpotential does not exceed 0.35 V) and 0.6−0.7 eV for the cathodic branch. The fit between the Marcus DOS theory and the Tafel data is generally excellent. In the pH range of 2−8 (Figure 7, pH = 4.0), the fit of the anodic branch to Marcus DOS theory is also excellent, with λ approximately 0.8 eV. However, the fit of the cathodic branch to theory is significantly worse, with λ approximately 0.5 eV. The cathodic branch tends to be linear with overpotential, and the slope of

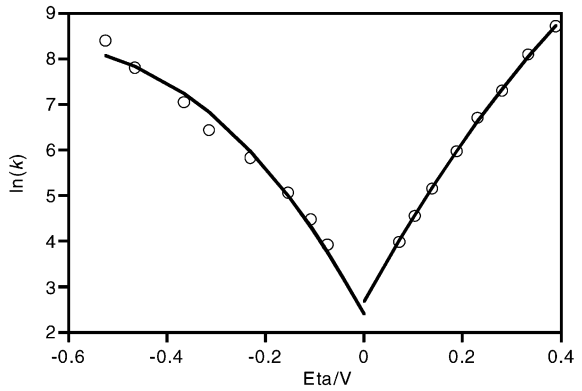

Figure 7. Tafel plot of ln(k_s) vs overpotential η at pH 4.0. The solid line is the least-squares fit to the Marcus density-of-states model with $\lambda = 0.85$ eV for the anodic branch and $\lambda = 0.45$ eV for the cathodic branch. The anodic intercept is 2.69 ($k_s = 15$ s^{-1}), and the cathodic intercept is 2.41 ($k_s = 11$ s^{-1}).

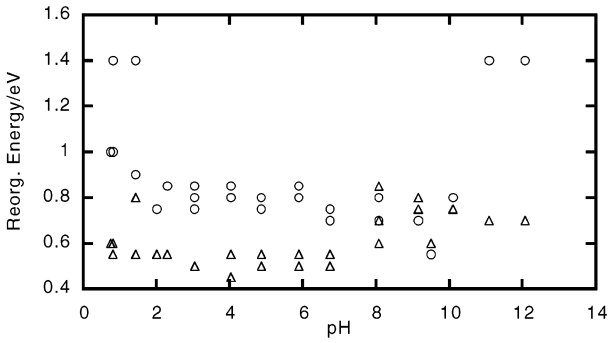

Figure 8. Anodic (circles) and cathodic (triangles) reorganization energies vs pH from fitting Tafel plots to the Marcus density-of-states model.

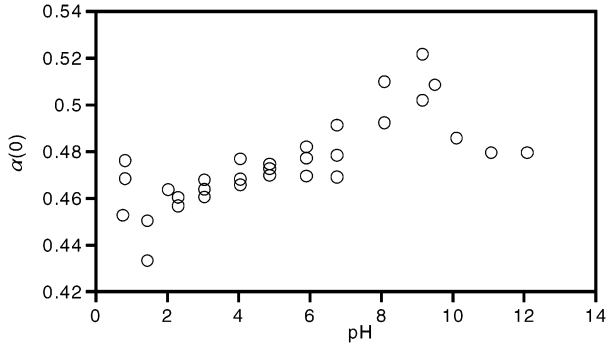

Figure 9. α(0) vs pH extracted from Tafel data.

the Tafel line is smaller than expected for simple electron transfer. In the pH range 8−10, the Tafel plots become nearly symmetrical, with anodic and cathodic reorganization energies equal to 0.7−0.8 eV.

The Tafel plot data are converted to a plot of the transfer coefficient α vs overpotential η as discussed in the Experimental Section. At all pHs, α increases with increasing η. A linear regression line is used to fit the data at overpotentials whose magnitude is less than 0.25 V. The fit yields both α(0) (intercept at $\eta = 0$) and a k_s value. The plot of log(k_s) vs pH (not shown) is similar to Figure 5, but with lower values for the standard rate constant (20 s^{-1} at low and high pH, 10−15 s^{-1} at intermediate pHs). The lower standard rate constants by these data analyses is a manisfestation of kinetic heterogeneity in the monolayer and is typical of all redox couples examined by this experimental method. In Figure 9, α(0) is plotted as a function of pH. Except for a narrow region around pH 8−10, α(0) is slightly below 0.5 at all pHs. Again, these results are consistent with the asymmetry in the Tafel plots (as indicated by the apparent reorganization energies for the anodic and cathodic branches, Figure 8) and in the peak splitting plot (Figure 4).

Discussion

Thermodynamically, the attached Os redox center with the water ligand exhibits the expected behavior for a 1*e*1H system. The standard potentials and pK_a values are in reasonable agreement with data on the unattached complex and the values reported by Takeuchi et al.[67] This redox center permits a kinetic study of all three pH regimes (low, intermediate, and high).

Kinetically, the Os 1*e*1H redox system exhibits substantial deviations from the stepwise model. First, at low (<2.4) and high (>9.3) pH, the anodic reorganization energy is substantially larger than the cathodic reorganization energy (Figure 8). At these pHs, the system should be exhibiting pure electron transfer with the water ligand either protonated or deprotonated in both oxidation states. Consequently, the reorganization energy should be same for the anodic and cathodic processes (as it is for both the Os chloride complex and the Ru complex studied previously). Second, and most dramatic, the plot of log(k_s) vs pH does not exhibit the deep minimum predicted by the model (Figure 5). Third, α(0) does not show the dramatic swings below 0.5 below mid pH and above 0.5 above mid pH (Figure 1) but is consistently below 0.5 (in the range 0.44−0.48) at all pHs except around pH 8−10, where it rises to 0.49−0.52 (Figure 9). The contrast with the kinetic behavior of the galvinol redox center is also striking. The galvinol redox centers exhibited a standard rate constant with strong pH dependence and α(0) significantly above 0.5 for a wide range of pHs.

Possible causes for the deviations from the stepwise model are experimental artifacts caused by *iR* drop and double-layer effects. Because the redox centers are attached to the electrode, the conversion of voltammetry data to rate constants does not depend on the sweep rate. The data analysis procedure requires only that the overpotential for a given rate constant be corrected for the *iR* drop. The low coverage of the Os redox centers and the high ionic strength of the electrolyte minimizes that correction. The *iR* drop only becomes significant (greater than 10 mV) at the highest scan rates (500 and 1000 V/s). Double-layer effects are discounted because of the nearly constant formal potential and kinetic parameters (k_s and λ) for the chloride analogue (which exhibits pure electron transfer) at all pHs.

The alternative to the stepwise model is the concerted transfer of the proton and electron. Concerted proton−electron transfer has been the focus of recent attention in terms of theory[72−77] and experiment for homogeneous systems.[78−82] A major manifestation of the concerted electron−proton transfer is the isotope effect. Replacing the proton with deuterium ion slows the kinetics of charge transfer dramatically in some systems.[78;79] The isotope effect would be nonexistent in the stepwise model when proton transfer is not rate limiting. There is one report of an isotope effect for PCET of a redox center attached to an electrode via a self-assembled monolayer, although the nature of the overall charge transfer step may be more complex than PCET.[83] However, there is no prediction yet in the literature on the pH and potential dependence of the standard rate constant for a concerted electron−proton transfer. It would be interesting to see whether theoretical predictions could account for the two major observations about the kinetics of the Os 1*e*1H system, the standard rate constant being nearly independent of pH and the Tafel plots showing the same asymmetry (anodic branch having a steeper slope than the cathodic branch) over most of

the pH range. The near symmetry in Tafel plots ($\alpha(0)$ close to 0.5) at pH 8−10 also needs an explanation.

The second question is whether concerted electron−proton transfer can account for the different behavior of the Os aquo complex and the previously studied galvinol system. The standard rate constant is strongly dependent on pH in the galvinol system, and $\alpha(0)$ is well above 0.5 over a wide range of pHs below pK_{a2}. The major anomaly in the galvinol system is a positive deviation of the log(k_s) plot vs pH from theory at pH less than 8. It seems possible that both a concerted and a stepwise mechanism could be operating, with the dominance of either mechanism depending on the nature of the redox center. Galvinol has widely separated pK_a values (pK_{a1} is estimated to be very negative, while pK_{a2} is approximately 13), indicating that electronic coupling between the site of electron transfer and the site of proton transfer is strong. On the other hand, the difference in pK_a values in the Os aquo complex is only about 7, suggesting a weaker coupling between the sites (electron transfer at the Os atom, proton transfer at the aquo ligand). Possibly the strong electronic coupling between electron and proton transfer sites (widely separated pK_a values) favors the stepwise model, while weak electronic coupling favors the concerted transfer model.

Many more experiments are needed to understand the causes of the deviations from the predictions of the stepwise model and to check the hypothesis of concerted electron−proton transfer. Two experiments that immediately come to mind are measurement of the isotope effect (repeat the experiments in D_2O) and variation in the chain length of the self-assembled monolayer to manipulate the standard rate constants for the pure electron transfers. The consequences of competing mechanisms on more complex systems (especially the important 2*e*2H systems, such as quinones and catechols) would also be interesting.

Conclusions

$[Os(II)(bpy)_2(4\text{-AMP})(Cl)]^+$ and $[Os(II)(bpy)_2(4\text{-AMP})(H_2O)]^{2+}$ redox centers have been attached to self-assembled monolayers on electrodes and their thermodynamic and kinetic behavior examined as a function of pH. The behavior of the Os chloride complex indicates that double-layer effects are negligible even though the monolayer contains an acidic moiety (COOH). The thermodynamic behavior of the Os aquo complex is consistent with a 1*e*1H redox system, and both formal potentials and acid dissociation constants are measured. The kinetic behavior of the Os aquo complex deviates substantially from the predictions of a stepwise proton−electron transfer model, a model that is widely used in the electrochemical literature to analyze proton-coupled electron transfer at electrodes. The deviations are tentatively attributed to concerted proton−electron transfer, which may either dominate the kinetic behavior or operate in parallel with stepwise proton−electron transfer.

References and Notes

(1) Brevnov, D. A.; Finklea, H. O.; Van Ryswyk, H. *J. Electroanal. Chem.* **2001**, *500*, 100−107.

(2) Finklea, H. O.; Ravenscroft, M. S.; Snider, D. A. *Langmuir* **1993**, *9*, 223−227.

(3) Finklea, H. O.; Hanshew, D. D. *J. Am. Chem. Soc.* **1993**, *114*, 3173−3181.

(4) Finklea, H. O.; Liu, L.; Ravenscroft, M. S.; Punturi, S. *J. Phys. Chem.* **1996**, *100*, 18852−18858.

(5) Finklea, H. O. *Electroanal. Chem.* **1996**, *19*, 109−335.

(6) Finklea, H. O.; Ravenscroft, M. S. *Isr. J. Chem.* **1997**, *37*, 179−184.

(7) Finklea, H. O.; Yoon, K.; Chamberlain, E.; Allen, J. *J. Phys. Chem. B* **2000**, *105*, 3088−3092.

(8) Finklea, H. O. In *Encyclopedia of Analytical Chemistry*; Meyers, R. A., Ed.; Wiley: New York, 2000; pp 10090−10115.

(9) Ravenscroft, M. S.; Finklea, H. O. *J. Phys. Chem.* **1994**, *98*, 3843−3850.

(10) Chidsey, C. E. D. *Science* **1991**, *251*, 919−922.

(11) Sachs, S. B.; Dudek, S. P.; Hsung, R. P.; Sita, L. A.; Smalley, J. F.; Newton, M. D.; Feldberg, S. W.; Chidsey, C. E. D. *J. Am. Chem. Soc.* **1997**, *119*, 10563−10564.

(12) Sikes, H. D.; Smalley, J. F.; Dudek, S. P.; Cook, A. R.; Newton, M. D.; Chidsey, C. E. D.; Feldberg, S. W. *Science* **2001**, *291*, 1519−1523.

(13) Smalley, J. F.; Feldberg, S. W.; Chidsey, C. E. D.; Linford, M. R.; Newton, M. R.; Liu, Y.-P. *J. Phys. Chem.* **1995**, *99*, 13141−13149.

(14) Creager, S. E.; Wooster, T. T. *Anal. Chem.* **1998**, *70*, 4257−4263.

(15) Curtin, L. S.; Peck, S. R.; Tender, L. M.; Murray, R. W.; Rowe, G. K.; Creager, S. E. *Anal. Chem.* **1993**, *65*, 386−392.

(16) Hockett, L. A.; Creager, S. E. *Langmuir* **1995**, *11*, 2318−2321.

(17) Richardson, J. N.; Peck, S. R.; Curtin, L. S.; Tender, L. M.; Terrill, R. H.; Carter, M. T.; Murray, R. W.; Rowe, G. K.; Creager, S. E. *J. Phys. Chem.* **1995**, *99*, 766−772.

(18) Sumner, J. J.; Creager, S. E. *J. Am. Chem. Soc.* **2000**, *122*, 11914−11920.

(19) Sumner, J. J.; Weber, K. S.; Hockett, L. A.; Creager, S. E. *J. Phys. Chem. B* **2000**, *104*, 7449−7454.

(20) Sumner, J. J.; Creager, S. E. *J. Phys. Chem. B* **2001**, *105*, 8739−8745.

(21) Weber, K. S.; Creager, S. E. *J. Electroanal. Chem.* **1998**, *458*, 17−22.

(22) Chambers, J. Q. In *The Chemistry of Quinonoid Compounds;* Patai, S., Rappoport, Z., Eds.; John Wiley: New York, 1988; Vol. II, pp 719−757.

(23) Albery, J. *Electrode Kinetics*; Oxford University Press: London, 1975; pp 125−163.

(24) Laviron, E. *J. Electroanal. Chem.* **1980**, *109*, 57−67.

(25) Laviron, E. *J. Electroanal. Chem.* **1981**, *124*, 1−7.

(26) Laviron, E. *J. Electroanal. Chem.* **1981**, *124*, 9−17.

(27) Laviron, E. *J. Electroanal. Chem.* **1982**, *134*, 205−212.

(28) Laviron, E. In *Electroanalytical Chemistry*; Bard, A. J., Ed.; Marcel Dekker: New York, 1982; pp 53−157.

(29) Laviron, E.; Roullier, L. *J. Electroanal. Chem.* **1983**, *157*, 7−18.

(30) Laviron, E. *J. Electroanal. Chem.* **1983**, *146*, 15−36.

(31) Laviron, E. *J. Electroanal. Chem.* **1983**, *146*, 1−13.

(32) Laviron, E. *J. Electroanal. Chem.* **1984**, *169*, 23−28.

(33) Laviron, E. *J. Electroanal. Chem.* **1984**, *169*, 29−46.

(34) Laviron, E. *J. Electroanal. Chem.* **1984**, *164*, 213−217.

(35) Finklea, H. O. *J. Electroanal. Chem.* **2001**, *495*, 79−86.

(36) Finklea, H. O. *J. Phys. Chem. B* **2001**, *105*, 8685−8693.

(37) Katz, E.; Schmidt, H.-L. *J. Electroanal. Chem.* **1993**, *360*, 337−342.

(38) Katz, E.; Schmidt, H.-L. *J. Electroanal. Chem.* **1994**, *368*, 87−94.

(39) Lahav, M.; Katz, E.; Willner, I. *Langmuir* **2001**, *17*, 7387−7395.

(40) Katz, E. Y.; Borovkov, V. V.; Evstigneeva, R. P. *J. Electroanal. Chem.* **1992**, *326*, 197−212.

(41) Hong, H.-G.; Park, W.; Yu, E. *J. Electroanal. Chem.* **1999**, *476*, 177−181.

(42) Hong, H.-G.; Park, W. *Langmuir* **2001**, *17*, 2485−2492.

(43) Ohtsuka, T.; Nagata, M.; Komori, H.; Nango, M. *Electrochemistry* **1999**, *67*, 1184−1186.

(44) Mukae, F.; Takemura, H.; Takehara, K. *Bull. Chem. Soc. Jpn.* **1996**, *69*, 2461−2464.

(45) Mo, Y.; Sandifer, M.; Sukenik, C.; Barriga, R. J.; Soriaga, M.; Scherson, D. *Langmuir* **1995**, *11*, 4626−4628.

(46) Yoshimoto, S.; Hirakawa, N.; Nishiyama, K.; Taniguchi, I. *Langmuir* **2000**, *16*, 4399−4404.

(47) Caldwell, W. B.; Chen, K.; Herr, B. R.; Mirkin, C. A.; Hulteen, J. C.; Van Duyne, R. P. *Langmuir* **1994**, *10*, 4109−4115.

(48) Caldwell, W. B.; Campbell, D. J.; Chen, K.; Herr, B. R.; Mirkin, C. A.; Malik, A.; Durbin, M. K.; Dutta, P.; Huang, K. G. *J. Am. Chem. Soc.* **1995**, *117*, 6071−6082.

(49) Campbell, D. J.; Herr, B. R.; Hulteen, J. C.; Van Duyne, R. P.; Mirkin, C. A. *J. Am. Chem. Soc.* **1996**, *118*, 10211−10219.

(50) Wang, R.; Iyoda, T.; Tryk, D. A.; Hashimoto, K.; Fujishima, A. *Langmuir* **1997**, *13*, 4644−4651.

(51) Evans, S. D.; Johnson, S. R.; Ringsdorf, H.; Williams, L. M.; Wolf, H. *Langmuir* **1998**, *14*, 6436−6440.

(52) Kondo, T.; Kanai, T.; Uosaki, K. *Langmuir* **2001**, *17*, 6317−6324.

(53) Tamada, K.; Nagasawa, J.; Nakanishi, F.; Abe, K.; Ishida, T.; Hara, M.; Knoll, W. *Langmuir* **1998**, *14*, 3264−3271.

(54) Wang, Y.-Q.; Yu, H.-Z.; Cheng, J.-Z.; Zhao, J.-W.; Cai, S.-M.; Liu, Z.-F. *Langmuir* **1996**, *12*, 5466−5471.

(55) Wolf, H.; Ringsdorf, H.; Delamarche, E.; Takami, T.; Kang, H.; Michel, B.; Gerber, C.; Jaschke, M.; Butt, H.-J.; Bamberg, E. *J. Phys. Chem.* **1995**, *99*, 7102−7102.
(56) Yu, H.-Z.; Wang, Y.-Q.; Cheng, J.-Z.; Zhao, J.-W.; Cai, S.-M.; Inokuchi, H.; Fujishima, A.; Liu, Z.-F. *Langmuir* **1996**, *12*, 2843−2848.
(57) Yu, H.-Z.; Wang, Y.-Q.; Cai, S.-M.; Liu, Z.-F. *Chem. Lett.* **1996**, 903−904.
(58) Yu, H.-Z.; Zhang, H.-L.; Liu, Z.-F.; Ye, S.; Uosaki, K. *Langmuir* **1998**, *14*, 619−624.
(59) Yu, H.-Z.; Zhang, J.; Zhang, H.-L.; Liu, Z.-F. *Langmuir* **1999**, *15*, 16−19.
(60) Yu, H.-Z.; Ye, S.; Zhang, H.-L.; Uosaki, K.; Liu, Z.-F. *Langmuir* **2000**, *16*, 6948−6954.
(61) Yu, H. Z.; Zhao, J. W.; Wang, Y. Q.; Cai, S. M.; Liu, Z. F. *J. Electroanal. Chem.* **1997**, *438*, 221−224.
(62) Yu, H. Z.; Shao, H. B.; Luo, Y.; Zhang, H. L.; Liu, Z. F. *Langmuir* **1997**, *13*, 5774−5778.
(63) Finklea, H. O.; Haddox, R. M. *Phys. Chem. Chem. Phys.* **2001**, *3*, 3431−3436.
(64) Haddox, R. M.; Finklea, H. O. *J. Electroanal. Chem.* **2003**, *550*−*551*, 351−358.
(65) Shultz, D. A.; Tew, G. N. *J. Org. Chem.* **1994**, *59*, 6159−6160.
(66) Takeuchi, K. J.; Samuels, G. J.; Gersten, S. W.; Gilbert, J. A.; Meyer, T. J. *Inorg. Chem.* **1983**, *22*, 1407−1409.
(67) Takeuchi, K. J.; Thompson, M. S.; Pipes, D. W.; Meyer, T. J. *Inorg. Chem.* **1984**, *23*, 1845−1851.
(68) Buckingham, D. A.; Dwyer, F. P.; Goodwin, H. A.; Sargeson, A. M. *Aust. J. Chem.* **1964**, *17*, 325−336.
(69) Kober, E. M.; Caspar, J. V.; Sullivan, B. P.; Meyer, T. J. *Inorg. Chem.* **1988**, *27*, 4587−4598.
(70) Dobson, J. C.; Takeuchi, K. J.; Pipes, D. W.; Geselowitz, D. A.; Meyer, T. J. *Inorg. Chem.* **1986**, *25*, 2357−2365.
(71) Smith, C. P.; White, H. S. *Langmuir* **1993**, *9*, 1−3.
(72) Decornez, H.; Hammes-Schiffer, S. *J. Phys. Chem. A* **2000**, *104*, 9370−9384.
(73) Hammes-Schiffer, S. *Acc. Chem. Res.* **2001**, *34*, 273−281.
(74) Soudachov, A. V.; Hammes-Schiffer, S. *J. Chem. Phys.* **1999**, *111*, 4672−4687.
(75) Soudachov, A. V.; Hammes-Schiffer, S. *J. Chem. Phys.* **2000**, *113*, 2385−2396.
(76) Cukier, R. I.; Nocera, D. G. *Annu. Rev. Phys. Chem.* **1998**, *49*, 337−369.
(77) Cukier, R. I. *J. Phys. Chem. B* **2002**, *106*, 1746−1757.
(78) Huynk, M. H. V.; White, P. S.; Meyer, T. J. *Angew. Chem., Int. Ed. Engl.* **2000**, *39*, 4101−4104.
(79) Huynk, M. H. V.; Meyer, T. J. *Angew. Chem., Int. Ed.* **2002**, *41*, 1395−1398.
(80) Lebeau, E. L.; Binstead, R. A.; Meyer, T. J. *J. Am. Chem. Soc.* **2001**, *123*, 10535−10544.
(81) Roth, J. P.; Lovell, S.; Mayer, J. M. *J. Am. Chem. Soc.* **2000**, *122*, 5486−5498.
(82) Weatherly, S. C.; Yang, I. V.; Thorp, H. H. *J. Am. Chem. Soc.* **2001**, *123*, 1236−1237.
(83) Murgida, D. H.; Hildebrandt, P. *J. Am. Chem. Soc.* **2001**, *123*, 4062−4068.